Available online at www.sciencedirect.com
SCIENCE DIRECT®
Pattern Recognition Letters 26 (2005) 2282–2294
Pattern Recognition Letters
www.elsevier.com/locate/patrec

Detection of cracks in computer tomography images of logs

Suchendra M. Bhandarkar [a], Xingzhi Luo [a,*], Richard Daniels [b], E. William Tollner [c]

[a] Department of Computer Science, The University of Georgia, Athens, Georgia 30602-7404, USA
[b] Warnell School of Forest Resources, The University of Georgia, Athens, Georgia 30602-2152, USA
[c] Department of Biological and Agricultural Engineering, The University of Georgia, Athens, Georgia 30602-4435, USA

Received 3 February 2005
Available online 9 August 2005

Communicated by R. Davies

Abstract

Computer Tomography (CT) is being increasingly employed for automated detection and localization of internal defects in logs prior to their sawing. Reliable detection and localization of cracks in CT images of logs is particularly important from the viewpoint of lumber production planning since the presence of cracks substantially reduces the value and also compromises the structural strength of the resulting lumber. A crack is hard to detect in a cross-sectional CT image of a log because it has geometric properties and grayscale values that are similar to those associated with the ring structure of the log. In this paper, a method for crack detection is presented, which exploits the fact that the line defining the crack makes a significant non-zero angle with the log ring structure. Sobel-like operators are used to extract both, the line defining the crack and the contours corresponding to the grayscale valleys between two neighboring rings. Fork detection and grouping methods are subsequently employed to localize the actual crack line using a RANSAC-based line fitting procedure. Experimental results show the advantages of the proposed technique for crack detection when compared to techniques that employ straightforward grayscale histogram-based thresholding.

Keywords: Crack detection; Computer tomography; Log scanning; Lumber production planning; Internal defect detection; Internal log defects

1. Introduction

Identification and localization of internal log defects is estimated to lead to potential gains of about 15%–18% in lumber value, representing

* Corresponding author. Tel.: +1 706 583 0613; fax: +1 706 542 2966.
E-mail address: xingzhi@cs.uga.edu (X. Luo).

0167-8655/$ - see front matter © 2005 Elsevier B.V. All rights reserved.
doi:10.1016/j.patrec.2005.04.004

a savings of over $2 billion for the hardwood lumber industry in the United States (Richards, 1977; Wagner et al., 1989). Computer Tomography (CT) is being increasingly employed for automated detection and localization of internal defects in logs prior to their sawing (Bhandarkar et al., 1999, 2002; Pham and Alock, 1998; Sarigul et al., 2003). A sequence of cross-sectional CT images of a log from one end to the other is obtained using a CT scanner and subsequently analyzed for the presence and locations of internal defects. Economic studies have shown that for large sawmills producing greater than 60×10^3 m^3 of lumber annually, an investment of about $1 million in CT scanning systems could be profitable even with only moderate increases (5%–10%) in lumber value yield (Hodges et al., 1990).

Automated detection and localization of cracks in the CT images of logs is particularly important from the viewpoint of lumber production planning since the presence of cracks substantially reduces the value and also compromises the structural strength of the resulting lumber (Bhandarkar et al., 1999). Failure to detect a crack may result in the production of unacceptable or low-quality lumber whereas the detection of a false crack may result in a suboptimal lumber production strategy where high-quality wood is wasted (Bhandarkar et al., 2002). The speed of crack detection is critical in a real-time production environment, as in an actual sawmill, since several CT images of a single log need to be processed in a timely manner. In our experiments, four CT image data sets from four hardwood logs (each 4 m long) are used. These hardwood logs are from three popular and widely used hardwood species in the United States (Ash, Maple and Oak) and are labeled as *Ash1*, *Ash2*, *Maple* and *Oak* respectively. The CT images of the logs are captured using a Toshiba TCT 20AX CT scanner (a third generation CT scanner) with a pixel resolution of 0.75 mm × 0.75 mm, an intensity resolution of 8 bits per pixel (i.e., 256 gray levels) and an image size of 316×316 pixels. The scanning of a 4 m log results in 224 cross-sectional CT images.

Automatic detection of cracks in a cross-sectional CT image of a log is particularly difficult because the geometric features and grayscale values associated with a crack are quite similar to those associated with areas between the annular rings of the log. This problem is exacerbated when the CT scanner has limited spatial resolution, in which case the high intensity values of the rings influence the grayscale values of the pixels representing the crack area. As a result, the grayscale values of the pixels representing the crack area are no longer as dark as anticipated. Hence a crack detection technique that is based solely on grayscale values of the image pixels (such as histogramming and grayscale-based thresholding) usually fails to detect the real cracks.

A crack, in a CT image of a log, is usually long and thin. A straightforward grayscale histogram-based binarization of the image results in the spatial fragmentation of the detected cracks. Although there are several papers in the literature that address defect detection in CT images of logs in general (Bhandarkar et al., 1999, 2002; Butler et al., 1989, 1993; Coates et al., 1998; Funt and Bryant, 1987; Pham and Alock, 1998; Sarigul et al., 2003), very few provide specific details on the technique(s) used to detect cracks. Moreover, the few crack detection techniques explicitly described in the literature are very specific to a certain mode of image capture and the types of features used, and hence not portable across systems. Bhandarkar et al. (1999, 2002) describe a grayscale histogram-based thresholding technique to detect cracks in cross-sectional CT images of logs. The choice of the grayscale threshold is based on the assumption that a crack is composed of a void volume that is filled largely by air instead of wood. On account of the lower material density of air compared to wood, the pixels in the CT image that represent cracks have much lower grayscale values than the other pixels. However, there is an inherent problem in threshold selection. Due to the finite resolution of the CT scanner, the grayscale values associated with the ring structure in the spatial proximity of the crack, often combine with the grayscale values of the pixels associated with the crack. This causes some of the pixels representing the crack to have a grayscale value that is much higher than that associated with a void volume. Thus, a threshold value that is close to the grayscale value associated with

a void volume results in several pixels associated with a crack to be classified as non-crack pixels thereby causing spatial fragmentation of the region containing the crack defect. In order to ensure that most of the cracks are detected, a threshold value much higher than the grayscale value associated with a void volume is used in practice (Bhandarkar et al., 1999). However, when the log is dry (i.e., has a low moisture content), the grayscale values of the pixels representing the areas between the rings is very close to the grayscale values of the pixels representing the cracks. A high threshold value causes these inter-ring areas to be incorrectly classified as cracks. Note that the detection of false cracks cannot be alleviated by using a higher resolution CT scanner. On the contrary, using a higher resolution CT scanner is not only expensive but also increases the computational complexity of the defect detection process on account of the increased CT image size.

Daut and Zhao (1993) propose a technique for detection of cracks in TV tubes using morphological operators. A crack, in this case, is usually long and thin, whereas noisy artifacts are usually round in shape. Thus, the medial axes (i.e., skeletons) of the shapes extracted using morphological operators are used to classify them as cracks or noisy artifacts. Nieniewski (1997) and Nieniewski et al. (1999) present a method for crack detection in ferrites. Morphological operators in the horizontal and vertical directions are used to enhance the cracks while exploiting the grayscale values of the crack-containing areas in the image. This method produces a result very similar to the commonly used grayscale-based binarization method. Consequently, the extracted crack features are fragmented and hard to distinguish from the noisy artifacts. A nearest neighbor (NN) classifier is needed to distinguish crack features from noisy artifacts, making the system computationally complex. Also, since the morphological operators are restricted to the horizontal and vertical directions, crack features which are neither horizontal nor vertical are difficult to detect. Mari et al. (1997) use similar morphological operators in their work in crack detection in images of ferrite cores.

Wu et al. (2003) propose a structural filtering method to detect creases in a fingerprint image. A crease has a structure that is very similar to that of a crack in a cross-sectional CT image of a log. In a fingerprint image, a crease can be geometrically modeled as a straight line. Moreover, a crease has the same grayscale value as the valleys between successive ridges in a fingerprint image (Fig. 1). The valleys in a fingerprint image, when viewed locally, can be looked upon as a collection of parallel lines. Both, the creases and the valleys have a higher grayscale value than the ridges (Fig. 1). A fundamental assumption in the structural filtering method is that the line defining a crease forms a certain non-zero angle with the set of parallel lines defining the valleys. This assumption is used directly in the design of the structural filters. The filtering technique searches in 12 different directions in order to match the structure within each local window to the predefined filters and consequently, has high computational complexity.

In the context of cross-sectional CT images of logs, a crack feature being thin and long, like a crease feature in a fingerprint image, can also be modeled as a line. The valleys between the rings in a cross-sectional CT image of a log are very similar to the valleys in a fingerprint image and hence can also be modeled locally as a set of parallel lines. We also assume that the line defining a crack feature forms a certain angle with the parallel lines that locally define the valleys. This assumption is supported by the work described in (Mairinger, 2003), which observes that in wooden panels, the cracks are oriented primarily in a direction that is perpendicular to the wood grain structure. We have verified this fact with all the cross-sectional CT images of logs that were available to us.

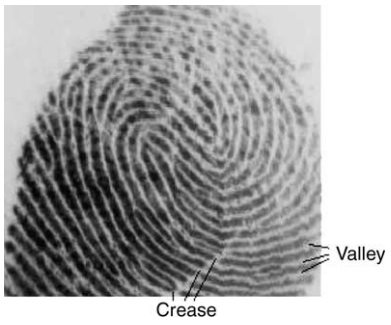

Fig. 1. A valley and crease in a fingerprint image.

The proposed crack detection scheme can be summarized as follows. The local linear structures resulting from cracks and valleys are first detected. Since the lines defining the cracks and the lines defining the local structure of the valleys intersect each other, the points of intersection can be represented as *fork* pixels within a local window. By detecting and localizing these fork pixels, the crack features can be actually detected and localized. In order to reject false crack features, which are usually caused by the presence of random noise between the rings, it is determined whether or not the detected crack feature is parallel to the local structure of the valleys. If the detected crack feature is parallel to the local structure of the valleys then it is discarded else it is retained as an actual crack feature.

In order to detect the lines associated with the crack features, four directional Sobel-like operators are used. These operators are observed to detect and localize reliably the linear features in a CT image, even in the presence of noise. These operators perform a combination of direction-sensitive smoothing and edge detection for linear features. They can detect the crack features without causing them to be fragmented. In addition to the crack features, the valleys between the rings are detected as well. A thinning algorithm is used to skeletonize the results of the Sobel-like operators. Fork pixels are then detected and localized within a 7×7 window. The fork pixels that are distributed along the same crack feature are grouped together, Groups of fork pixels that are parallel to the local ring or valley structure are discarded. The algorithm for grouping fork pixels is based on connectivity and mutual proximity of the fork pixels. It exploits the fact that fork pixels on the same crack should be spatially proximate and connected to each other.

The organization of the remainder of the paper is as follows. In Section 2, the methods for preliminary detection of potential crack features and binarization of the resulting image are described. In Section 3, a method for grouping the fork pixels and detecting the crack features using a line fitting method is described. In Section 4, the technique used to distinguish between true crack features and noisy artifacts is described. In Section 5, experimental results of the proposed technique on cross-sectional CT images of hardwood logs are presented and compared with results obtained using grayscale histogram-based thresholding. In Section 6, the paper is concluded and the directions for future research are outlined.

2. Edge detection and binarization

Fig. 2(a) shows the raw cross-sectional CT image of a hardwood log in which a crack feature is obviously visible. The grayscale value of a void area, as given by a typical CT scanner with an 8 bits per pixel grayscale resolution (i.e., 256 distinct gray levels in the range 0–255), is in the range 3–4. However when a threshold value of 10 is chosen to binarize the image, the crack feature is spatially fragmented as shown in Fig. 2(b). Raising the threshold to 50, results in the inclusion of several non-crack pixels from the ring structure of the dry portion of the log as shown in Fig. 2(c). As the threshold value is raised, the grayscale valleys between successive rings get increasingly visible. As a consequence, it is not possible to separate the grayscale valleys from the crack features using a simple grayscale-based thresholding technique. The work in this paper does not try to separate the crack pixels from the grayscale valley pixels using the grayscale values alone; instead, a feature-based method is used. An edge detector is used to extract both, the potential crack features and the grayscale valleys between rings. Subsequent structural analysis is then used to identify and localize the true crack lines.

Given that the crack features are usually thin and long, four Sobel-like edge operators are used to detect potential crack features based on their linearity property. These four operators are termed as OP_x, OP_y, OP_{xy} and OP_{yx} (Fig. 3). Using these four edge operators, four edge images E_x, E_y, E_{xy} and E_{yx} are generated using Eq. (1), where $\otimes$ denotes the convolution operation.

$$\begin{aligned} E_x(i,j) &= \mathrm{OP}_x \otimes I(i,j) \\ E_y(i,j) &= \mathrm{OP}_y \otimes I(i,j) \\ E_{xy}(i,j) &= \mathrm{OP}_{xy} \otimes I(i,j) \\ E_{yx}(i,j) &= \mathrm{OP}_{yx} \otimes I(i,j) \end{aligned} \tag{1}$$

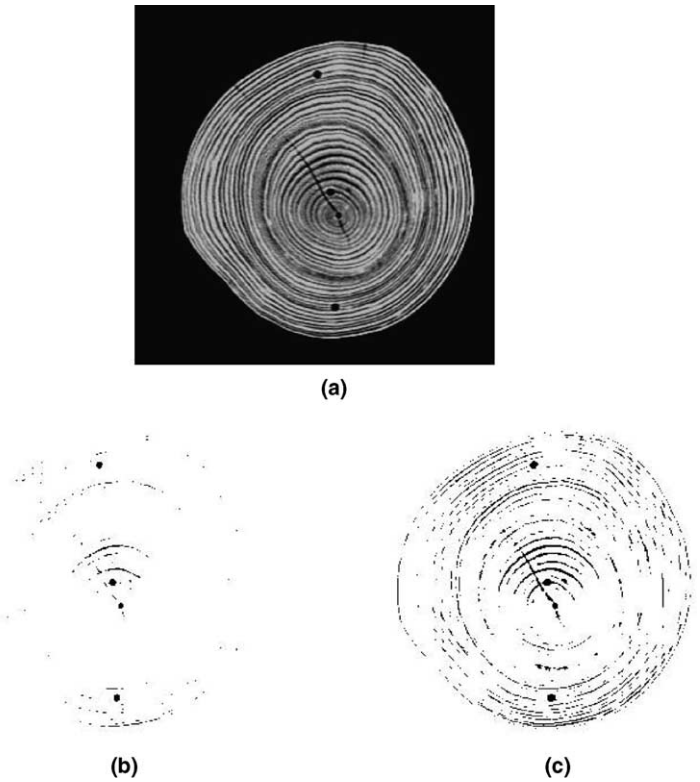

Fig. 2. Original CT image and the results of grayscale-based thresholding: (a) original CT image, (b) result with threshold = 10 and (c) result with threshold = 50.

Each of the four operators can be decomposed into two suboperators where one suboperator serves as an edge detector along a specified direction and the other serves as smoothing operator along a direction perpendicular to the direction of the edge detector. For example, the operator OP_x can be decomposed into two suboperators $OP_x = OP_{xe} \otimes OP_{xs}$ as shown in Fig. 4. The operator decomposition serves to speed up the computation.

The final edge image is a composition of the four edge images

$$E(i,j) = \max(E_x(i,j), E_y(i,j), E_{xy}(i,j), E_{yx}(i,j)); \quad (2)$$

Given that a crack feature typically has a much lower grayscale value when compared to other log features, the $E(i,j)$ value corresponding to a crack pixel should be much larger than zero in the resulting edge image E. A simple thresholding method is used to binarize the edge image. The edge image resulting from the four Sobel-like operators is shown in Fig. 5 whereas the binary edge image is shown in Fig. 6. It can be noticed that both the crack lines and the grayscale valleys between the rings are clearly visible in the binary edge image.

The Hough Transform (HT) is a popular technique for detection of linear features in images and could potentially be used for crack detection in CT images of logs. However, the HT was observed to perform poorly when used for crack detection in the binary edge images due to the interference of features arising from the grayscale valleys between the rings. Fig. 7 depicts the HT image (in parameter space) of the binary edge image in Fig. 6. As Fig. 7 shows, it is difficult to identify the peaks in the HT image corresponding to the linear crack defects in the presence of inter-

1	1	1	1	1
0	0	0	0	0
-2	-2	-2	-2	-2
0	0	0	0	0
1	1	1	1	1

(a)

1	0	-2	0	1
1	0	-2	0	1
1	0	-2	0	1
1	0	-2	0	1
1	0	-2	0	1

(b)

0	0	0	0	1	0	0
0	0	0	1	0	-2	0
0	0	1	0	-2	0	1
0	1	0	-2	0	1	0
1	0	-2	0	1	0	0
0	-2	0	1	0	0	0
0	0	1	0	0	0	0

(c)

0	0	1	0	0	0	0
0	-2	0	1	0	0	0
1	0	-2	0	1	0	0
0	1	0	-2	0	1	0
0	0	1	0	-2	0	1
0	0	0	1	0	-2	0
0	0	0	0	1	0	0

(d)

Fig. 3. The four Sobel-like operators for edge detection: (a) horizontal operator OP_x, (b) vertical operator OP_y, (c) diagonal operator OP_{xy} and (d) diagonal operator OP_{yx} .

1	1	1	1	1
0	0	0	0	0
-2	-2	-2	-2	-2
0	0	0	0	0
1	1	1	1	1

=

1
0
-2
0
1

⊗

1	1	1	1	1

Fig. 4. Example of operator decomposition.

Fig. 5. Raw edge image obtained using the four Sobel-like operators.

feature interference. The problem is further exacerbated when the line segments delineating the crack features are short in length. The HT coupled with local analysis and morphological reconstruction

Fig. 6. Binary edge image.

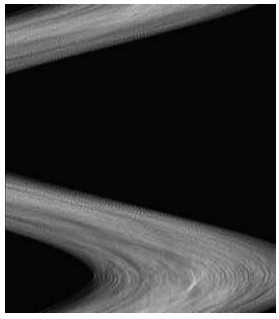

Fig. 7. Hough Transform image from the binary edge image.

in the image space could conceivably be used to extract the crack defects reliably, but would prove to be extremely time consuming. Also note that morphological operators are typically sensitive to the presence of noisy artifacts in the input data.

3. Edge thinning and fork detection

Edge thinning and minutiae detection have been widely discussed in fingerprint recognition and verification (Jain et al., 1997; Maio and Maltoni, 1997; Prabhakar et al., 2000; Ratha et al., 1995). In this paper, the thinning algorithm proposed by Cychosz (1994) is used on the binary edge image. The result of the thinning algorithm on the binary edge image in Fig. 6 is shown in Fig. 8. In the binary thinned edge image, the 1 pixels represent edge pixels and 0 pixels represent non-edge pixels.

As is evident in Figs. 6 and 8, a potential crack feature typically intersects the ring structure of the log resulting in the creation of *forks* at the points of intersection. These forks have the same structure as *minutiae* in fingerprint images (Jain et al., 1997; Maio and Maltoni, 1997; Prabhakar et al., 2000; Ratha et al., 1995). It is reasonable to localize the crack features by detecting the fork pixels in the thinned image. A simple and efficient minutiae detection method using a 3×3 window is discussed in (Jain et al., 1997). Let $N_1, \ldots, N_8$ be the binary values (0 or 1) of the eight neighboring pixels of a given center pixel with value 1. The center pixel is classified as a ridge bifurcation (a class of minutiae) in the context of fingerprint image analysis if $\sum_{i=1}^{8} N_i > 2$. The detection of ridge bifurcations in fingerprint images is analogous to the detection of fork pixels in cross-sectional CT images of logs. To make the fork detection process more robust, a 7×7 window is used to remove false fork pixels. If the center pixel of a 7×7 window, is a true fork pixel, it should extend three or more branches to the border of the window. However, if two branches are too close to each other, they are counted as one. Fig. 9 shows two candidate fork pixels P_1 and P_2 being analyzed. Both P_1 and P_2 have three neighboring 1 pixels and four branch pixels located on the border of the window. However in the case of pixel P_1, border pixels 1 and 2 are close to each other and so are border pixels 3 and 4. This is a typical case caused by the ring structure of the log. If pixels 2 and 4 are deleted because of their proximity to pixels 1 and 3 respectively, then pixel P_1 has only two branch pixels on the border of the 7×7 window. Hence P_1 is considered a false fork pixel and removed from further consideration. Using the same analysis, P_2 is retained as a candidate fork pixel. With the above analysis, a large number of false fork pixels ($75\% \sim 85\%$ in our experiments) can be removed which makes the subsequent analysis more efficient. Fig. 10 shows the results of the fork pixel detection procedure.

The analysis described above cannot remove false fork pixels between the rings when the rings are seriously smeared due to the finite resolution of the CT scanner. Hence the candidate fork pixels are grouped using a clustering algorithm and the overall structure of the grouped pixels is analyzed to verify whether they are located along or perpendicular to the log ring structure. Prior to the clustering operation, the distance between each pair of

Fig. 8. Result of the thinning algorithm.

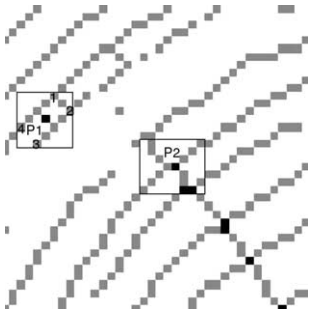

Fig. 9. Candidate fork pixel detection in a 7×7 window.

Fig. 10. Result of false fork pixel suppression by analysis of border pixels.

fork pixels is computed. For two fork pixels to be placed within the same group, they must be located within the same crack feature area. This can be checked by testing whether or not there exists a path composed entirely of 1 pixels (i.e., a 1-path) connecting the two candidate fork pixels. As shown in Fig. 11, there exists no such 1-path between candidate fork pixels P_1 and P_2, and hence they cannot be placed in the same group. However, since there exists a 1-path between candidate fork pixels P_2 and P_3, they can be placed in the same group. A 1-path between two candidate fork pixels is determined by performing a depth-first search within a local window containing the two candidate fork pixels. The depth-first search algorithm to verify the connectivity between two 1-pixels p_1 and p_2 is described as follows:

(1) Mark pixel p_1 and push it onto an empty stack.
(2) Pop the topmost pixel p_t from the stack. For each of its 8-neighboring pixels p, if p is p_2, then there exists a 1-path between pixels p_1 and p_2, hence stop. Otherwise, if pixel p is in the local window centered at pixel p_t, has not been marked and has value 1, push pixel p onto the stack and mark it.
(3) Repeat step (2) iteratively. If pixel p_2 is not encountered in step (2) and the stack is empty, then there is no 1-path between pixels p_1 and p_2.

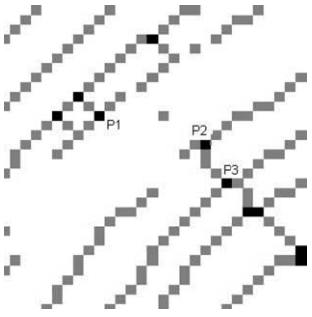

Fig. 11. Grouping of candidate fork pixels.

In order to speed up the clustering process, a distance table between the candidate fork pixels is established. The distance table is initialized with the Euclidean distance between every pair of fork pixels. If the Euclidean distance between a pair of fork pixels is $\leqslant a$ threshold T (in our case $T = 10$), then the existence of a 1-path between the two candidate fork pixels is verified using the above depth-first search algorithm. If there exists a 1-path between the two candidate fork pixels then the value of the Euclidean distance between them, as computed earlier, is retained in the distance table. In the absence of a 1-path between the two candidate fork pixels, the corresponding entry in the distance table is set to a very large value (theoretically ∞) since the candidate fork pixels are deemed not to lie within the same crack feature area. Since that the presence or absence of a 1-path connecting two candidate fork pixels is verified only when the Euclidean distance between them is less than T (i.e., they are close together), the distance table can be generated quickly.

The candidate fork pixels are grouped using the following greedy algorithm. Here, F is an array of the candidate fork pixels where $F[i]$ denotes the ith fork pixel, N is the number of candidate fork pixels, and T_{num} is the minimum number of fork pixels within a group.

(1) for $i = 0$ to N do
  (a) Create an empty set G, and add candidate fork pixel $F[i]$ to G.
  (b) for $j = i + 1$ to N, if fork pixel $F[j]$ is at a distance $< T$ from any fork pixel $\in G$, then add $F[j]$ to G.
(2) If the number of fork pixels $\in G \geqslant T_{\text{num}}$, then save set G. For each fork pixel $\in G$, set its distance from any other fork pixel $\notin G$ to

a very high value so that the fork pixels $\in G$ will not be considered when creating subsequent groups.

The application of the above grouping scheme to the candidate fork pixels depicted in Fig. 10, results in the retention of a single group of candidate fork pixels as shown in Fig. 12. This is the desired group of true fork pixels. Note that path connectivity is implicit in the construction of the distance table.

However, candidate fork pixels may be detected between the rings of the log when these rings are close to each other or when they are smeared in the CT image. Fig. 13 depicts some groups of false fork pixels which are distributed along the ring structure. Since it is reasonable to assume that the crack feature forms a finite angle with the local ring structure, these false groups of candidate fork pixels can be eliminated using the following geometric analysis.

In order to eliminate false groups of candidate fork pixels which are actually parallel to the local ring structure, the direction of the tangent to the local ring structure in the vicinity of the group of candidate fork pixels is determined. It is assumed that the annular rings in the cross-sectional CT image of the log can be modeled as concentric circles with their common center at the centroid of the log cross-section. Thus, the direction of the tangent to local ring structure can be easily evaluated. Fig. 14 provides a closer look at a group of false candidate fork pixels located along the local ring structure. A line L_1 is fitted to the group of candidate fork pixels using the RANSAC line fitting procedure (Fischler and Bolles, 1981) described briefly in the following section. The centroids P_1 and O of the group of candidate fork pixels and the log cross-section respectively are computed. The tangent L_2 to the local ring structure is approximated as being perpendicular to the line OP_1. The group of candidate fork pixels is deemed to be spurious if the angle between L_1 and L_2 is very small (i.e., below a certain threshold value), else the group of candidate fork pixels is deemed to represent a true crack feature.

Fig. 12. Results of the grouping procedure.

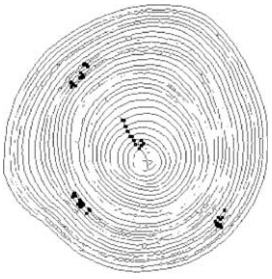

Fig. 13. Results of the grouping procedure depicting false candidate fork pixels.

4. Crack area extraction

The grouping technique described above enables localization of the fork pixels along the line describing the crack feature. However, the number of fork pixels is not large enough to ensure robust line extraction, especially when the line segment delineating the crack defect is short in length. This also provides a justification for grouping the fork pixels instead of applying the HT directly to all

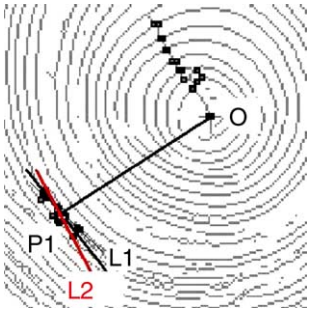

Fig. 14. Removal of a group of false candidate fork pixels.

the fork pixels in order to extract the line segments delineating the crack defects. Note that the robustness of the HT decreases as the ratio of the data (fork) pixels to noisy (non-fork) pixels decreases. In order to ensure robust line extraction, in addition to the fork pixels within a group, the pixels between the fork pixels in the skeletonized (i.e., thinned) image are considered as well. The candidate fork pixels within a group are ordered and the bounding box for the group is computed. If the width of the bounding box is larger than the height, the candidate fork pixels in the group are ordered along the x axis, otherwise they are ordered along the y axis. If $\{p_i\}$ is the ordered set of candidate fork pixels within the group, then for each pair of successive fork pixels (p_i, p_{i+1}), a local window can be defined by using the pixels (p_i, p_{i+1}) as the corner points of the window. The 1-pixels in the skeletonized image obtained from all the windows, thus defined for every pair of successive candidate fork pixels along with the fork pixels, are used in the line extraction procedure.

When the pixels associated with the crack are known, the HT or a simple linear regression method can be used to extract the line representing the crack. The HT is more robust to outliers than straightforward linear regression which attempts to compute a minimum-mean-squared-error (MMSE) fit to the underlying data and is easily confounded by outliers. However, linear regression is computationally much faster than the HT which entails an exhaustive search of the parameter space for each data point. In this paper the RANSAC algorithm (Fischler and Bolles, 1981) is used to perform the line fitting since it offers both, computational efficiency and robustness to outliers. The RANSAC algorithm randomly (or exhaustively) samples a subset of points from the given set of data points to perform MMSE-based line fitting. The data points whose distances from the fitted line are above a certain threshold are considered as outliers whereas the remaining data points are considered to be inliers. If the number of inliers is above a certain percentage of the total number of data points, the MMSE-based line fitting is performed again but the input data points are restricted to the inlier set. If the inlier set is not large enough, the above procedure is repeated on a new subset of the input data points. The three aforementioned techniques for linear feature extraction (HT, linear regression and RANSAC) were compared on 150 crack feature data sets collected from cross-sectional CT images of the four sample hardwood logs described in Section 1. The number of data points in each data set ranged from 30 to 200 points. The average run time per data set on a 2.0 GHz Pentium workstation with 2.0 GB of RAM was observed to be 1.11 ms for the HT, 3.28 ms for simple linear regression, and 2.10 microseconds for the RANSAC-based algorithm. Thus the RANSAC-based algorithm was observed to be much faster than the HT and equally robust to outlier data. The result of the RANSAC-based algorithm is depicted in Fig. 15.

The parameters of the fitted line are used to identify the pixels in the binary image that belong to the actual crack feature. This is to account for the fact that the line segment defined by the fork pixels may be shorter than the actual crack feature since the ring structure is often weak in the vicinity of the center of the log cross-section, causing fork pixels to go undetected. Thus, if a 1-pixel in the binary image belongs to the actual crack feature, then it must be both, close enough to the fitted line and also spatially connected, via a 1-path, to the fork pixels within the group. The following iterative depth-first search procedure is used to localize the actual crack pixels.

(1) Push all the fork pixels onto a stack as seeds.
(2) Pop the uppermost pixel from the stack and store it in pixel P.

Fig. 15. The result of the RANSAC-based line fitting to the detected fork pixels.

(3) If the distance of pixel P from the fitted line is less than a threshold T_d, then
   (a) Mark pixel P as a crack pixel.
   (b) Check the 8-neighborhood of pixel P in the binary image. If any of its 8-neighboring pixels is a 1-pixel, then push it onto the stack.
(4) Perform steps (2) and (3) until the stack is empty.

The result of the above depth-first search procedure is depicted in Fig. 16.

5. Experimental results

For the purpose of comparison, the grayscale histogram-based crack detection and localization procedure described in (Bhandarkar et al., 1999) was performed on the CT image slice shown in Fig. 2(a) and the result is depicted in Fig. 17. As is evident, the grayscale histogram-based crack extraction procedure incorrectly classifies the grayscale valleys between successive rings as crack features. A visual comparison of the results in Figs. 16 and 17 clearly demonstrates the limitations of the grayscale histogram-based crack extraction procedure.

Figs. 18 and 19 depict the results of the proposed crack extraction procedure on two other CT images. From the results, it can be seen that the four Sobel-like operators are capable of accurate detection and localization of the linear features in the image which aids in the extraction of potential crack features. The procedures for detection and grouping of fork pixels and the subsequent RANSAC-based line fitting to the detected fork pixels enable the estimation of the parameters of the line that best describes the crack feature. Pixels from the grayscale valleys between successive rings, that are incorrectly classified as belonging to crack features based on their grayscale values, are eliminated using geometric analysis. Note that the RANSAC-based line fitting proce-

Fig. 16. Identification and localization of the actual crack defect.

Fig. 17. Results of the grayscale histogram-based crack extraction procedure.

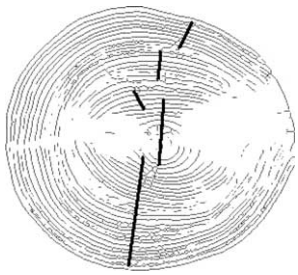

Fig. 18. Results of the proposed crack detection procedure on the second CT image.

Fig. 19. Results of the proposed crack detection procedure on the third CT image.

Table 1
Experimental results

	Ash1	Ash2	Maple	Oak
Run time (s)	24	21	21	20
Time/frame (s)	0.107	0.094	0.094	0.089
Total cracks	112	22	21	0
Correct identification	105 (94%)	21 (99%)	19 (90%)	0
False negatives	7 (6%)	1 (5%)	2 (10%)	0
False positives	10 (9%)	2 (9%)	1 (5%)	0

dure is also capable of rejecting outliers in the input data.

Experimental results on cross-sectional CT images from the aforementioned four hardwood logs are tabulated in Table 1. The results of the crack detection procedure were compared with those obtained from a human expert grader examining the physically sawed lumber. The detection rate was observed to be $\geqslant 90\%$ with a false negative rate (miss rate) $\leqslant 10\%$ and false positive rate (false detection rate) $\leqslant 9\%$. The overall processing speed was observed to be $\leqslant 30$ s for a 4-m long hardwood log on a 2.0 GHz Pentium workstation with 2.0 GB of RAM.

6. Conclusions and future work

In this paper, a method for crack detection in cross-sectional CT images of logs was presented. The proposed method exploits the fact that the line defining the crack makes a significant non-zero angle with the log ring structure. Sobel-like operators were used to extract both, the line defining the crack and the contours corresponding to the grayscale valleys between two successive rings. Fork detection and grouping methods were subsequently employed to localize the actual crack line using a RANSAC-based line fitting procedure. Experimental results demonstrated the advantages of the proposed technique for crack detection when compared to techniques that employ straightforward grayscale histogram-based thresholding.

Although the technique described in the paper focused on detection of cracks in CT images of hardwood logs, it can be ported to other problem domains (with some modifications) where linear features need to be extracted in the presence of noisy artifacts and inter-feature interference. Detection of fractures in the human rib cage and detection of creases or scars in fingerprint images are two problem domains where proposed technique could be used. The basic elements of the proposed technique, namely, (a) detection of fork pixels, (b) elimination of false fork pixels caused by noisy artifacts and inter-feature interference using geometric analysis that exploits the structural relationship between the feature of interest and the interfering features, and (c) RANSAC-based robust line fitting to extract the linear feature of interest, would be applicable in these problem domains as well. Future research will examine the application of the proposed technique to these problem domains. Although the proposed technique can analyze a 4-meter log for the presence of cracks in less than 30 seconds, further improvements in speed are desirable to make suitable for real-time deployment in an actual sawmill. The use of parallel processing and feature tracking across multiple CT image slices will be explored in this regard.

Acknowledgement

This research was supported in part by a NRICGP award by the US Department of Agriculture to Drs. Bhandarkar, Daniels and Tollner (Award Number 2001-35103-10049).

References

Bhandarkar, S.M., Faust, T.D., Tang, M., 1999. CATALOG: A system for detection and rendering of internal log defects using computer tomography. J. Machine Vision Appl. 11, 171–190.

Bhandarkar, S.M., Faust, T.D., Tang, M., 2002. Design and prototype development of a computer vision-based lumber production planning system. Image Vision Comput. 20, 167–189.

Butler, D.A., Brunner, C.C., Funck, J.W., 1989. A dual-threshold image sweep-and-mark algorithm for defect detection in veneer. Forest Products J. 39 (5), 25–28.

Butler, D.A., Brunner, C.C., Funck, J.W., 1993. An adaptive image processing algorithm for defect defection in douglar-fir veneer. Forest Products J. 43 (5), 57–60.

Coates, E.R., Chang, S.J., Liao, T.W., 1998. A quick defect detection algorithm for magnetic resonance images (MRI) of hardwood logs. Forest Products J. 48 (10), 68–74.

Cychosz, J.M., 1994. Efficient binary image thinning using neighborhood maps. Graphics Gems IV. Academic Press, pp. 465–473.

Daut, D.G., Zhao, D., 1993. A flaw detection method based on morphological image processing. IEEE Trans. Circuit Syst. Video Technol. 3 (6), 389–398.

Fischler, M., Bolles, R., 1981. Random sample consensus: A paradigm for model fitting with applications to image analysis and automated cartography. Commun. ACM 24 (6), 381–395.

Funt, B.V., Bryant, E.C., 1987. Detection of internal log defects by automatic interpretation of computer tomography images. Forest Products J. 37 (1), 56–62.

Hodges, D.G., Anderson, W.C., McMillin, C.W., 1990. The economic potential of CT scanners for hardwood sawmills. Forest Products J. 40 (3), 65–69.

Jain, A.K., Hong, L., Bolle, R., 1997. On-line fingerprint verification. IEEE Trans. Pattern Anal. Machine Intell. 19 (4), 302–314.

Maio, D., Maltoni, D., 1997. Direct gray-scale minutiae detection in fingerprints. IEEE Trans. Pattern Anal. Machine Intell. 19 (1), 27–40.

Mairinger, F., 2003. Strahlenuntersuchung an Kunstwerken. E.A. Seemann, Berlin, Germany.

Mari, M., Dambra, C., Chetverikov, D., Verestoy, J., Jozwik, A., Nieniewski, M., Chmielewski, L., Sklodowski, M., Cudny, W., Lugg, M., 1997. The crash project: defect detection and classification in ferrite cores. In: Proceedings of the 9th International Conference on Image Analysis and Processing., Vol. II. Springer-Verlag, Berlin.

Nieniewski, M., 1997. Morphological method for detecting defects on the surface of ferrite cores. In: Proceedings of the 10th Scandinavian Conference on Image Processing, Vol. I. Lappeenranta, Finland.

Nieniewski, M., Chmielewski, L., Jozwik, A., Sklodowski, M., 1999. Morphological detection and featured-based classification of cracked regions in ferrites. Machine Graphics Vision 8 (4), 699–712.

Pham, D.T., Alock, R.J., 1998. Automated grading and defect detection: a review. Forest Products J. 48 (4), 34–42.

Prabhakar, S., Jain, A.K., Wang, J., Pankanti, S., Bolle, R., 2000. Minutia Verification and Classification for Fingerprint Matching. In: International Conference Pattern Recognition, Barcelona, Spain, Vol. 1, September, pp. 1025–1030.

Ratha, N., Chen, S., Jain, A.K., 1995. Adaptive flow orientation based feature extraction in fingerprint images. Pattern Recog. 28 (11), 1657–1672.

Richards, D.B., 1977. Value yield from simulated hardwood log sawing. Forest Products J. 27 (12), 47–50.

Sarigul, E., Abbott, A.L., Schmoldt, D.L., 2003. Progress in analysis of computed tomography (CT) images of hardwood logs for defect detection. In: Proceedings of the Tenth International Conference on Scanning Technology and Process Optimization in the Wood Industry, ScanTech, Seattle, Washington, Nov., pp. 19–30.

Wagner, F.G., Taylor, F.W., Ladd, D.S., McMillin, C.W., Roder, F.L., 1989. Ultrafast CT scanning of an oak log for internal defects. Forest Products J. 39 (11/12), 62–64.

Wu, C., Zhou, J., Bian, Z., Rong, G., 2003. Robust Crease Detection in Fingerprint Images. In: Proceedings of the IEEE Computer Society Conference on Computer Vision and Pattern Recognition, Madison, Wisconsin, June Vol. II, pp. 505–512.